A Pyrene-based Platform for Studying the Relationship of Steric Effects on Optical Properties

Xinyi Song,[a#] Min Wang,[b#] Wei Liu,[a] Heng Zheng,[a] Carl Redshaw,[c] Xing Feng,[*a,d] Zujin Zhao, [*b] Ben Zhong Tang[*e]

[a] Guangdong Provincial Key Laboratory of Functional Soft Condensed Matter, School of Material and Energy, Guangdong University of Technology, Guangzhou 510006, China.

[b] State Key Laboratory of Luminescent Materials and Devices, Guangdong Provincial Key Laboratory of Luminescence from Molecular Aggregates, South China University of Technology, Guangzhou, 510640, P. R. China.

[c] Chemistry, School of Natural Sciences, University of Hull, Hull, Yorkshire HU6 7RX, UK.

[d] Guangdong Provincial Key Laboratory of Luminescence from Molecular Aggregates (South China University of Technology), Guangzhou 510640, P. R. China.

[e] School of Science and Engineering, Shenzhen Institute of Aggregate Science and Technology, The Chinese University of Hong Kong, Shenzhen, Guangdong 518172, China.

Abstract: Triphenylamine is a weak fluorophore with an aggregation-caused quenching (ACQ) effect. By integrating the pyrene and different substituents (such as benzene, pyrene, phenylcarbazole, tetraphenylethylene (TPE)), a set of new pyrene-based triphenylamine (TPA) analogues have been prepared in order to understand the stereoscopic effects on the emission behavior both in solution and in the solid state. The compounds which contain the pyrene unit (such **Py2Ph**, **2PyPh** and **PyCz**) can improve the fluorescence but still exhibit an ACQ feature, while the TPE decorated compound **PyTPE** exhibited a typical aggregation-induced emission (AIE) characteristic. Moreover, the degree of π-conjugation and the electronic effects can affect the molar absorbance coefficients. Due to the stereoscopic effect of these TPA analogues, the

emission compounds show slight changes before and after grinding. Furthermore, due to their good thermal stability and quantum yields, the compounds **PyCz** and **PyTPE** were selected as light emitting layers for fabricating organic light emitting diodes (OLEDs) which exhibited good electroluminescence properties.

Keywords: pyrene, steric effect, organic light-emitting diode, aggregation-induced emission, structure-properties relationship

Introduction

High-performance organic π-conjugated luminescent materials in the solid-state have been widely utilized in optoelectronic devices, such as organic light-emitting diodes (OLEDs), [1],[2] organic field effect transistors (OFETs) etc. [3] Due to spontaneous self-assembly into an aggregate, the luminescent materials exhibit opposite emission behavior, *i.e.*, aggregation-caused quenching (ACQ) phenomenon and aggregation-induced emission (AIE) phenomenon. [4] The aggregates undergo an ACQ effect and can form strong inter-/intra-molecular interactions (such as π-π stacking, hydrogen-bond etc.) resulting in emission quenching. [5] While the typical AIE molecules display weak or non-emissive behavior in solution, the emission can be enhanced in the aggregated state. [6] AIE luminogens (AIEgens) have attracted much attention which is attributed to their highly efficient optical properties in the solid-state. [7] Thus, how to suppress the π-π stacking and overcome the drawbacks of the ACQ effect, or realize the ACQ to AIE transformation, to achieve high-efficiency solid-state luminescent materials remains a challenge. [8]

The key feature to modulate the luminescent materials for high emission in the solid-state is to adjust the weak inter-/intramolecular interactions. For example, hydrogen bonding can play an important role to strengthen the intermolecular interactions, and when the hydroxyl group was replaced by methoxyl, the quantum yield was increased from 0.04 to 0.75. [9] On the other hand, the 3D topological structure plays a crucial role in regulating the intermolecular interactions and arranging the molecular packing pattern. Triphenylamine (TPA) contains a central nitrogen atom with three phenyl rings to form a 3D propeller-like structure (C3 symmetry), resulting in a large steric

hindrance and good hole transport properties. [10] TPA is an aggregation-caused quenching (ACQ) moiety with strong electron-donating ability, [11] and modified TPA has been widely integrated into AIEgens for various applications such as biolabeling [12], [13] and organic light-emitting diodes etc. [14],[15]

Pyrene is an important family member of the PAHs, which have been attracting great attention both in organic synthesis, materials science and the industrial community, due to their high thermal stability, chemical stability, excellent ordered structure and unique photoelectric properties. [16],[17] Pyrene emits deep blue fluorescence (372 nm) and has a high quantum yield (0.64) in toluene. [18] However, due to the large π-conjugated backbone and planar structure, pyrenes tend to form dimers through π-π stacking at high concentration, leading to a fluorescence quenching. [19] Much effort has been devoted to the development of pyrene derivatives with high-efficiency fluorescence properties, via inhibiting the molecular aggregation by functionalizing the pyrene core or constructing excellent pyrene-based emitter with AIE features.[20],[19]

To suppress the π-π stacking of pyrene, it is a feasible approach to adjust the luminescent properties via functionalizing the pyrene core, or introducing a twist in the molecular structure via choosing or adjusting suitable moieties (such as the length of chain, the type and the steric effect of substituents), which provide diversified electronic push-pull properties or spatial steric hindrance, achieving excellent emission behavior.[20] So, this article attempts to integrate the advantages of the TPA unit to prepare a set of pyrene-based TPA analogues for understanding the influence of the steric effects on the optical behavior. Compared to TPA, the emission intensity of the pyrene-based TPA analogues has been enhanced with quantum yields of more than 0.40 in the solid state, exhibiting a good electroluminescence property, and the maximum emission peak and luminescence is 470 nm and 12710 cd m^{-2} respectively.

Experimental section

Materials

Unless otherwise stated, all reagents used were purchased from commercial sources and were used without further purification. The precursor and final compounds **Py2Ph**, **2PyPh**, **PyCz** and **PyTPE** were synthesized via a Buchwald–Hartwig amination reac-

tions under similar conditions in high yield.

Characterization

^{1}H and ^{13}C NMR spectra were recorded on a Bruker AV 400M spectrometer using chloroform-d solvent and tetramethylsilane as internal reference. J-values are given in Hz. High-resolution mass spectra (HRMS) were recorded on a LC/MS/MS, which consisted of a HPLC system (Ultimate 3000 RSLC, Thermo Scientific, USA) and a Q Exactive Orbitrap (QE orbitrap type) mass spectrometer. UV-vis absorption spectra and photoluminescence (PL) spectra were recorded on a Shimadzu UV-2600 and the Hitachi F-4700 spectrofluorometer. PL quantum yields were measured using absolute methods using a Hamamatsu C11347-11 Quantaurus-QY Analyzer. The quantum lifetime was recorded on an Edinburgh FLS 980 instrument and measured using a time-correlated single-photon counting method. Thermogravimetric analysis was carried on a Mettler Toledo TGA/DSC3+ under dry nitrogen at a heating rate of 10 ºC/min. The quantum chemistry calculation was performed on the Gaussian 09 (B3LYP/6–311G (d,p) basis set) software package.

X-ray Crystallography

Crystallographic data for the compounds was collected on a Bruker APEX 2 CCD diffractometer with graphite monochromated Mo Kα radiation (λ = 0.71073 Å) in the ω scan mode. [21] The structures were solved by charge flipping or direct methods algorithms and refined by full-matrix least-squares methods on F^2. [22,23] All esds (except the esd in the dihedral angle between two l.s. planes) were estimated using the full covariance matrix. The cell esds were considered individually in the estimation of esds in distances, angles and torsion angles. Correlations between esds in cell parameters were only used when they were defined by crystal symmetry. An approximate (isotropic) treatment of cell esds was used for estimating esds involving l.s. planes. The final cell constants were determined through global refinement of the xyz centroids of the reflections harvested from the entire data set. Structure solution and refinements were carried out using the SHELXTL-PLUS software package. The partially occupied water molecule of crystallization was modelled by the Platon Squeeze procedure. Data (excluding structure factors) on the structures reported here

have been deposited with the Cambridge Crystallographic Data Centre. CCDC 2261348 (**Py2Ph**), 2261350 (**PyCz**), 2261349 (**PyTPE**) contain the supplementary crystallographic data for this paper. These data can be obtained free of charge from The Cambridge Crystallographic Data Centre via www.ccdc.cam.ac.uk/data_request/cif.

Synthetic procedures

Synthesis of *N*,*N*-diphenylpyren-1-amine (Py2Ph)

Under a nitrogen atmosphere, a mixture of 1-bromopyrene (1) (200 mg, 0.71 mmol, 1.0 eq.), *N*,*N*-diphenylamine (144 mg, 0.85 mmol, 1.2 eq.), Cs_2CO_3 (1.16 g, 3.56 mmol, 5 eq.) and *t*-Bu_3P (528 mg, 2.67 mmol) in toluene (10 mL) solution was stirred for 10 min at room temperature. Then $Pd(OAc)_2$ (60 mg, 0.1 mmol) was added, and the mixture was heated to reflux for 48 h. After it was cooled, the mixture was quenched by H_2O (50 mL) and extracted by CH_2Cl_2 (50 mL× 3) three times. The combined organic layer was successively washed with water (30 mL) and brine (50 mL), and dried over $MgSO_4$ and evaporated. The residue was purified by column chromatography eluting with hexane to give *N*,*N*-diphenylpyren-1-amine (**Py2Ph**) and recrystallization in the mixed solution of dichloromethane and *n*-hexane (V_{CH2Cl2}:V_{hexane} = 1 : 2) to afford a light green crystalline sample (198 mg, 75%, melting point =185 ºC). ^{1}H NMR (400 MHz, $CDCl_3$) δ 8.20-8.16 (m, 2H), 8.15 (d, *J* = 9.9 Hz, 2H), 8.11 (d, *J* = 7.0 Hz, 1H), 8.06 (s, 2H), 7.98 (t, *J* = 7.6 Hz, 1H), 7.93 (d, *J* = 9.2 Hz, 1H), 7.83 (d, *J* = 8.1 Hz, 1H), 7.24 – 7.16 (m, 4H), 7.11 – 7.05 (m, 4H), 6.98 – 6.91 (m, 2H) ppm. ^{13}C NMR (100 MHz, $CDCl_3$) δ 148.8, 141.0, 131.3, 131.2, 129.6, 129.3, 128.3, 128.0, 127.8, 127.3, 127.2, 126.5, 126.3, 126.1, 125.3, 125.2, 124.9, 123.4, 122.2, 121.9 ppm. HRMS (FTMS + p APCI) m/z: [M+H]+ Calcd for $C_{28}H_{19}N$ 370.1518; Found, 370.1588.

***N*-phenyl-*N*-(pyren-1-yl)pyren-1-amine (2PyPh)**

Under a nitrogen atmosphere, a mixture of *N*-phenylpyren-1-amine (1) (200 mg, 0.68 mmol, 1.0 eq.), 1-bromopyrene (229 mg, 0.82 mmol, 1.2 eq.), Cs_2CO_3 (1.11 g, 3.41 mmol, 5 eq.) and *t*-Bu_3P (528 mg, 2.67 mmol) in toluene (10 mL) solution was stirred 10 min at room temperature. Then $Pd(OAc)_2$ (60 mg, 0.1 mmol) was added, and the mixture was heated to reflux for 48 h. After it was cooled, the mixture was quenched by H_2O (50 mL) and extracted by CH_2Cl_2 (50 mL× 3) three times. The combined

organic layer was successively washed with water (30 mL) and brine (50 mL), and dried over $MgSO_4$ and evaporated. The residue was purified by column chromatography (silica gel column) eluting with hexane to give a pale yellow powder **2PyPh** (125 mg, 37%, melting point= 356 °C). ^{1}H NMR (400 MHz, $CDCl_3$) δ 8.33 (d, *J* = 9.2 Hz, 2H), 8.17 (d, *J* = 7.6 Hz, 2H), 8.10 (d, *J* = 7.6 Hz, 2H), 8.07 (d, *J* = 8.2 Hz, 2H), 8.03 (s, 2H), 8.02 (s, 2H), 7.98 (t, *J* = 7.6 Hz, 2H), 7.91 (d, *J* = 9.3 Hz, 2H), 7.80 (d, *J* = 8.2 Hz, 2H), 7.15 (t, *J* = 7.9 Hz, 2H), 6.93 (d, *J* = 7.3 Hz, 1H), 6.83 (d, *J* = 7.9 Hz, 2H) ppm.^{13}C NMR (100 MHz, $CDCl_3$) δ 151.0, 142.4, 131.4, 131.1, 129.2, 129.0, 127.8, 127.3, 126.9, 126.8, 126.4, 126.3, 126.2, 125.8, 125.2, 125.0, 125.0, 123.5, 120.9, 120.4 ppm. HRMS (FTMS + p APCI) m/z: $[M+H]^+$ Calcd for $C_{38}H_{25}N$ 494.1903; Found, 494.1905.

***N*-(4-(*9H*-carbazol-9-yl)phenyl)-*N*-phenylpyren-1-amine (PyCz)**

Under a nitrogen atmosphere, a mixture of 4-(*9H*-carbazol-9-yl)-*N*-phenylaniline (1) (200 mg, 0.59 mmol, 1.0 eq.), 1-bromopyrene (198 mg, 0.71 mmol, 1.2 eq.), Cs_2CO_3 (960 mg, 2.95 mmol, 5 eq.) and *t*-Bu_3P (528 mg, 2.67 mmol) in toluene (10 mL) solution was stirred 10 min at room temperature. Then $Pd(OAc)_2$ (60 mg, 0.1 mmol) was added, and the mixture was heated to reflux for 48 h. After it was cooled, the mixture was quenched by H_2O (50 mL) and extracted by CH_2Cl_2 (50 mL× 3) three times. The combined organic layer was successively washed with water (30 mL) and brine (50 mL), and dried over $MgSO_4$ and evaporated. The residue was purified by column chromatography eluting (silica gel column) with *n*-hexane, affording a pale yellow powder and recrystallization in the mixed solution of dichloromethane and *n*-hexane (V_{CH2Cl2}:V_{hexane} = 2 : 1) produced light green crystalline **PyCz** (130 mg, 41%, melting point = 251 °C). ^{1}H NMR (400 MHz, $CDCl_3$) δ 8.24 (d, *J* = 8.8 Hz, 2H), 8.21 (d, *J* = 7.7 Hz, 1H), 8.16 (d, *J* = 7.6 Hz, 1H), 8.12 (d, *J* = 7.7 Hz, 1H), 8.09 (s, 1H), 8.03 (d, *J* = 9.6 Hz, 1H), 8.02 (d, *J* = 7.6 Hz, 1H), 7.42 (m, 3H), 7.36 d, J = 8.8 Hz, 2H), 7.31 – 7.19 (m, 9H), 7.01 (dd, *J* = 13.0, 5.9 Hz, 1H) ppm. ^{13}C NMR (100 MHz, $CDCl_3$) δ 148.3, 148.0, 141.2, 140.5, 131.3, 131.1, 130.8, 130.0, 129.5, 128.5, 128.3, 129.0, 127.8, 127.4, 127.3, 126.5, 126.4, 126.2, 125.9, 125.5, 125.3, 124.9, 123.3, 123.2, 122.8, 122.6, 122.2, 120.3, 119.8, 109.9 ppm. HRMS (FTMS + p APCI) m/z: [M+H]+ Calcd for $C_{40}H_{26}N_2$ 535.2169; Found, 535.2154.

***N*-phenyl-*N*-(4-(1,2,2-triphenylvinyl)phenyl)pyren-1-amine (PyTPE)**

Under a nitrogen atmosphere, a mixture of *N*-phenyl-4-(1,2,2-triphenylvinyl)aniline (1) (200 mg, 0.47 mmol, 1.0 eq.), 1-bromopyrene (159 mg, 0.57 mmol, 1.2 eq.), Cs_2CO_3 (766 mg, 2.35 mmol, 5 eq.) and *t*-Bu_3P (528 mg, 2.67 mmol) in toluene (10 mL) solution was stirred 10 min at room temperature. Then $Pd(OAc)_2$ (60 mg, 0.1 mmol) was added, and the mixture was heated to reflux for 48 h. After it was cooled, the mixture was quenched by H_2O (50 mL) and extracted by CH_2Cl_2 (50 mL× 3) three times. The combined organic layer was successively washed with water (30 mL) and brine (50 mL), and dried over $MgSO_4$ and evaporated. The residue was purified by column chromatography (silica gel column) eluting with *n*-hexane, affording a pale green powder and recrystallization in the mixed solution of dichloromethane and *n*-hexane (V_{CH2Cl2}:V_{hexane} =3 : 1) produced light green crystalline **PyTPE** (180 mg, 61%, melting point=221 ºC). ^{1}H NMR (400 MHz, $CDCl_3$) δ 8.20-8.11 (m, 3H), 8.08 (d, *J* = 9.2 Hz, 1H), 8.05 (s, 2H), 8.00 (t, *J* = 7.6 Hz, 1H), 7.94 (d, *J* = 9.3 Hz, 1H), 7.79 (d, *J* = 8.2 Hz, 1H), 7.23 – 7.00 (m, 19H), 6.93 (t, *J* = 7.3 Hz, 1H), 6.85 (d, *J* = 8.7 Hz, 2H), 6.79 (d, *J* = 8.7 Hz, 2H). ^{13}C NMR (100 MHz, $CDCl_3$) δ 148.5, 147.0, 144.1, 143.9, 143.7, 140.9, 140.8, 140.4, 137.2, 132.2, 131.4, 131.3, 131.1, 129.5, 129.2, 128.1, 127.7, 127.7, 127.6, 127.3, 127.1, 126.4, 126.4, 126.3, 126.3, 126.0, 125.2, 125.1, 123.5, 122.3, 121.9, 121.1 ppm. HRMS (FTMS + p APCI) m/z: $[M+H]^+$ Calcd for $C_{48}H_{33}N$ 624.2686; Found, 624.2687.

Results and discussion

Synthesis

To gain insight into the effect of steric properties on the optical behavior, a set of pyrene-based triphenylamine (TPA) analogues were synthesized via a Pd-catalyzed Buchwald–Hartwig reaction. The synthetic route and corresponding molecular structures are illustrated in Figure 1 and Scheme S1. One phenyl of the TPA unit was replaced by a pyrene (Py), *N*-phenylcarbazole (Cz) or tetraphenylethylene (TPE) unit to tune the molecular structure and steric effects, in order to modulate the optical bahavior, molecular morphology, as well as the

electroluminescence properties. Firstly, a Buchwald–Hartwig reaction of the aniline with the corresponding bromo-substituted compounds (such Py-Br, Cz-Br or TPE-Br) afforded the intermediates, which were further involved in a Buchwald-Hartwig reaction with 1-bromopyrene to afford **2PyPh**, **PyCz**, or **PyTPE** in high yield. For comparison, *N*,*N*-diphenylpyren-1-amine (**Py2Ph**) was synthesized as a control compound. All intermediates and target compounds were characterized by $^{1}H/^{13}C$ NMR spectroscopy and high-resolution mass spectrometry (HRMS), and the compounds **Py2Ph**, **PyTPE** and **PyCz** were also characterized by single crystal X-ray diffraction. The target compounds **Py2Ph**, **PyTPE** and **PyCz** display good solubility in common solvents, but **2PyPh** only dissolves in hot CH_2Cl_2 and $CHCl_3$.

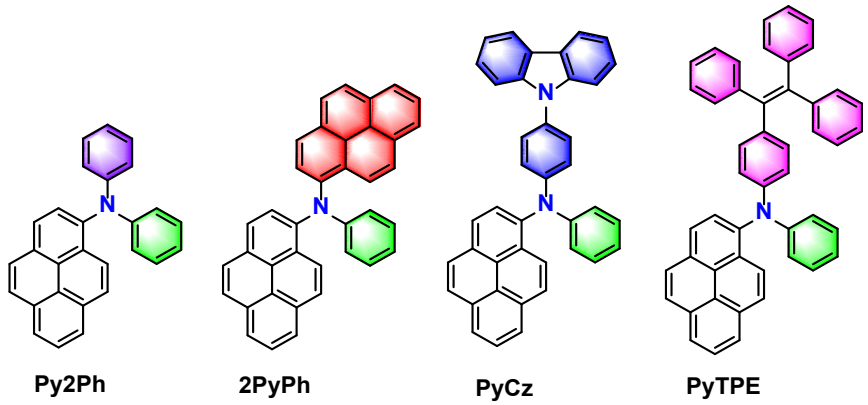

Figure 1. Molecular structures of the pyrene-based TPA analogues **Py2Ph**, **2PyPh**, **PyCz**, and **PyTPE**.

Thermal stability

The thermal stability of these compounds was investigated by thermogravimetric analysis (TGA) and is summarized in Figure S16. All compounds have good thermal stability with high decomposition temperatures of 312 °C for **Py2Ph**, 401°C for **2PyPh**, 423 °C for **PyCz**, and 410 °C for **PyTPE** (5% weight loss), respectively. The carbonization residue (coke yield) is also 1.7%, 0.5%, 0.8% and 1.1% respectively. In addition, when the temperature is about 177 °C, the compound **PyTPE** shows about a 4.5% weight loss, which may be attributed to the loss of captured solvent molecules. Meanwhile, the phase changes of these

compounds were studied by differential scanning calorimetry (DSC). As shown in Figure S17, the four compounds all have a high melting point, namely 185℃ for **Py2Ph**, 356℃ for **2PyPh**, 251℃ for **PyCz**, 221℃ for **PyTPE** and only **2PyPh** undergoes a glass transition at 221℃.

Photophysical properties

The UV-vis absorption and photoluminescence spectra of the four pyrene-based TPA analogues were measured in dilute THF solution (~10^{-5} M) at room temperature. As shown in Figure 2A, the compounds **Py2Ph**, **2PyPh**, **PyCz**, and **PyTPE** exhibited two similar absorption peaks in the range of 290-340 nm and 350-450 nm, respectively. The short-wavelength absorption band belongs to the π-π* transition, and the long-wavelength absorption band originates from the molecular n-π* transition. However, due to the different substituents, four compounds exhibited different molar absorbance coefficients (ε). Compared to the compound **Py2Ph**, compound **2PyPh** containing two pyrene moieties show the largest absorption coefficient constants (ε) in the long-wavelength absorption band with ε of 2.0×10^4 L M^{-1} cm^{-1}. Meanwhile, when the electron-donating ability of substituents increases, the ε of the short-wavelength absorption band increases from 2.3×10^4 L M^{-1} cm^{-1} (**Py2Ph**) to 3.2×10^4 L M^{-1} cm^{-1} for **PyTPE** and 3.5×10^4 L M^{-1} cm^{-1} for **PyCz** (Figure 2A). Clearly, the length of the π-conjugation of the substituent and the electronic effect can affect the absorption coefficients.

Table 1. The photophysical properties of pyrene-based derivatives.

Compd	ε ($\lambda_{max\ abs}$) (L M^{-1} cm^{-1})[a]	λ_{maxPL} (nm) soln[a]/solid[b]	Φ_f	τ (ns)	α_{AIE}[d]	K_r[e] ($\times10^7$ S^{-1})	K_{nr}[f] ($\times10^7$ S^{-1})
Py2Ph	298(2.3×10^4) 380(1.3×10^4)	462 / 496	0.69[a] 0.38[c] 0.30[b]	6.18[a] 3.76[c] 5.74[b]	0.43	0.1[a] 0.1[c] 0.06[b]	0.06[a] 0.166[c] 0.11[b]
2PyPh	318(2.1×10^4) 407(2.0×10^4)	478 / 486	0.63 0.20 0.21	4.71 1.54 1.56	0.33	0.13 0.13 0.12	0.08 0.519 0.52
PyCz	294(3.5×10^4) 380(1.2×10^4)	472 / 479	0.69 0.58 0.45	7.77 7.36 4.80	0.65	0.09 0.08 0.09	0.039 0.056 0.118
PyTPE	332(3.2×10^4) 382(1.8×10^4)	470 / 494	0.04 0.22	1.50 2.68	9.75	0.03 0.08	0.637 0.293

0.39	2.71	0.14	0.229

[a]Maximum emission wavelength of THF solution. [b]Maximum emission wavelength of solid state.[c] Measured in mixture of THF/water solution with f_w = 99%. [d]$\alpha = \Phi_{solid}/\Phi_{soln.}$ [e]k_r = radiative decay rate (Φ/τ). [f]k_{nr} = nonradiative decay rate ($1/\tau - k_r$).

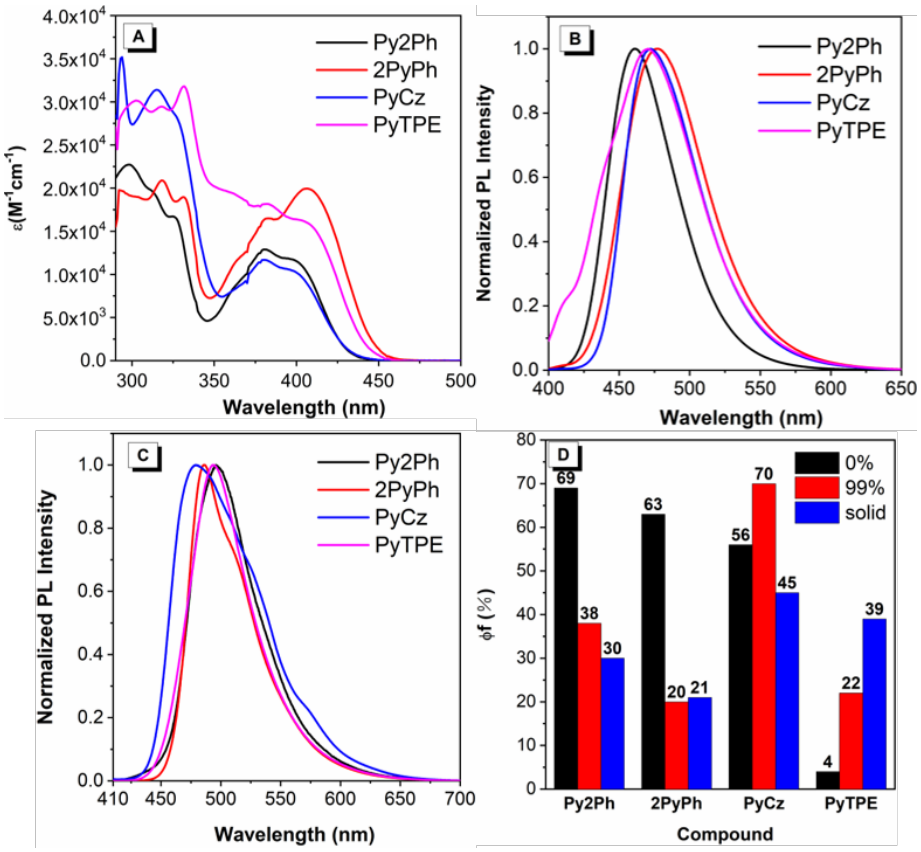

Figure 2. A): UV-Vis absorption spectra; B): PL spectra in THF (10^{-5} M) of compounds **Py2Ph**, **2PyPh**, **PyTPE** and **PyCz**; C) Emission spectra of four compounds in the solid state (λ_{ex} = 369 nm); D) Quantum yields of four compounds in solution (black (in THF) and red (water/THF in 99:1 ratio)) and solid state (blue).

Upon excitation, all compounds exhibit similar emission behavior in THF solution with maximum emission peaks at 462 nm (**Py2Ph**), 478 nm (**2PyPh**), 472 nm (**PyCz**), and 470 nm (**PyTPE**), respectively (Figure 2B, Table 1). Compared to the solution, all of these compounds exhibit a red-shift emission of 496 nm, 486 nm, 479 nm and 494 nm in the solid state, respectively. The large

red-shifted emission for **Py2Ph** and **PyTPE** maybe ascribe to the presence of strong π-π stacking between the pyrene rings. Four pyrene-based triphenylamine analogues show a large red-shifted emission of more than 120 nm compared to the triphenylamine ((λ_{ex} = 362nm in THF), indicating that the asymmetric molecular structure for the four compounds broke the electronic structure of the triphenylamine, resulting in a donating-accepting effect. The quantum yields of the four compounds were measured both in solution and in the solid state. As shown in Figure 2D, the compounds **Py2Ph**, **2PyPh** and **PyCz** exhibit a higher quantum yield (0.69 for **Py2Ph,** 0.63 for **2PyPh** and 0.69 for **PyCz**) in solution compared to in the solid state. As expected, the compound **PyTPE** containing a TPE unit shows a high quantum yield in the solid state (39%) compared to in solution (4%), indicated that the **PyTPE** may exhibit AIE characteristics.

Thus, the emission of the four pyrene-based TPA analogues **Py2Ph**, **2PyPh**, **PyCz** and **PyTPE** were examined in dilute THF and a mixture THF/H_2O with different water contents (f_w). Upon excitation, the TPA analogues **Py2Ph**, **2PyPh**, **PyCz** exhibit bright emission in THF solution. When the f_w was gradually increased from 0% to 99%, the molecules tend to form aggregates, leading to fluorescence intensity quenching with a slight red-shifted emission (483 nm for **Py2Ph**, 492 nm for **2PyPh** and 488 nm for **PyCz**). Indeed, the fluorescence quantum yield (ϕ_f) (0.38 for **Py2Ph**, 0.20 for **2PyPh** and 0.58 for **PyCz**) in the aggregate state (f_w = 99%) has decreased in varying degrees compared to those in THF solution. The calculated radiative decay rate (k_r) of **Py2Ph** and **2PyPh** is ~10^8 S^{-1} decreasing to 10^7 S^{-1}. The K_r of **PyCz** has slightly increased, while the nonradiative decay rate (k_{nr}) increased roughly more than 2-fold compared to in solution. Thus, the compounds **Py2Ph**, **2PyPh** and **PyCz** are indeed non-AIE active.

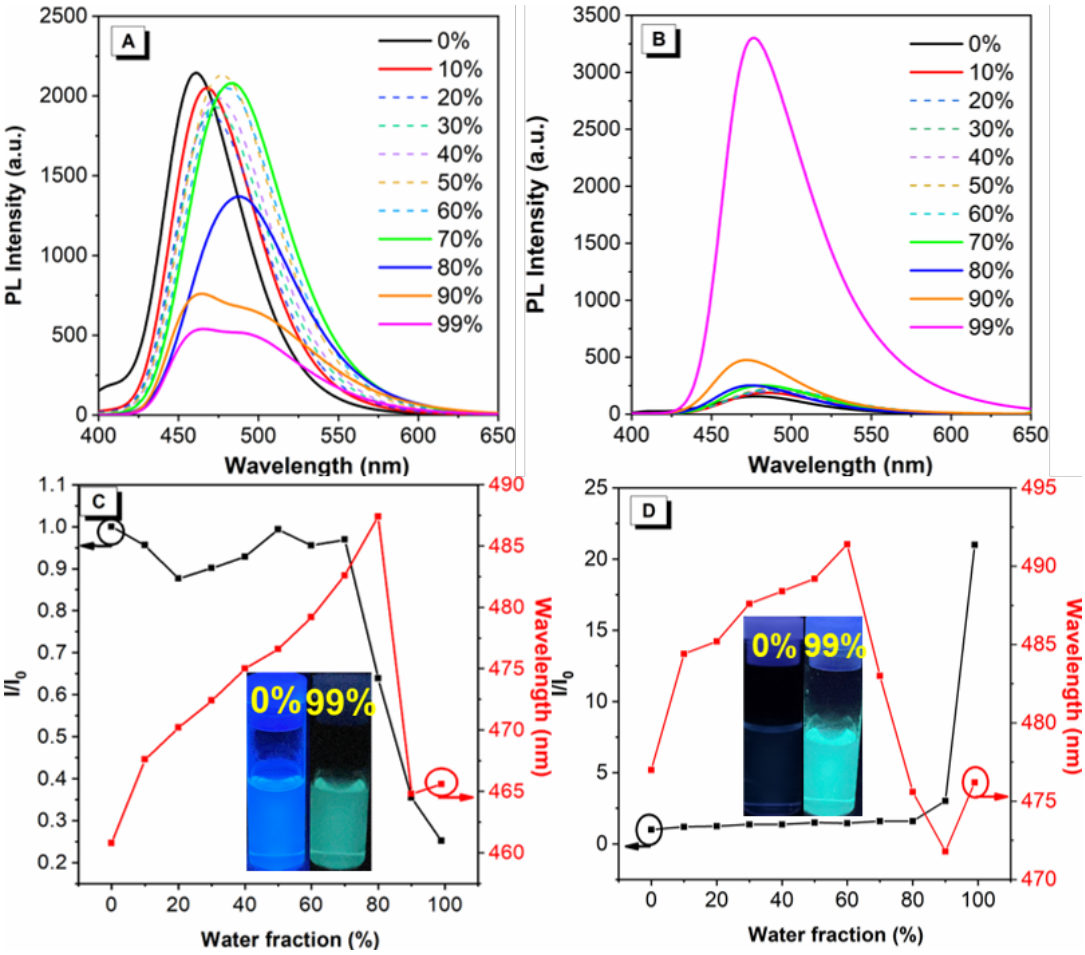

Figure 3. PL spectra of (A) **Py2Ph** and (B) **PyTPE** in THF/water mixtures with different water fractions (f_w) (≈10^{-5} M); C) D): Plot of relative PL intensity I/I_0. Inset: fluorescent images of **Py2Ph** and **PyTPE** in THF/water mixtures at different f_w (0% and 99%) taken under 365 nm UV irradiation.

Generally, the compounds containing the TPE unit exhibit typical AIE characteristics. Similarly, the compound **PyTPE** showed weak blue emission in THF solution, with a maximum emission peak at 470 nm. With the increase of f_w to 60%, the maximum emission peak was red-shifted to 491 nm, which is attributed to an intermolecular charge transfer (ICT) process. On further increasing f_w to 90%, the emission intensity significantly enhanced with a blue-shifted emission at 471 nm (Figure 3). A reasonable explanation for this phenomenon is the aggregated hydrophobic **PyTPE** molecules eliminate the effect of solvent polarity, resulting in a blue-shifted emission. [24][25] The Φ_f of **PyTPE** in solution was increased from 0.04 to

0.22 at f_w = 99%, and the fluorescence quantum lifetime (τ) was 1.50 ns in solution and increased to 2.71 ns in the solid state (Table 1). The calculated radiation delay rate (k_r) of **PyTPE** is 3×10^6 S^{-1} increasing to 1.4×10^8 S^{-1}, while the nonradiative decay rate (k_{nr}) decreased from 6.37×10^8 S^{-1} to 2.29×10^8 S^{-1}. So, the **PyTPE** containing TPE is AIE-active.

Solvatochromic effects

Based on our knowledge, pyrene may act as an electron-donating group or an electron-withdrawing group depending on the microenvironment. [26] Moreover, a substituent group can be introduced at the 1-position of pyrene, which can increase the electronic communication between the pyrene and the substituents.[27] In order to study the effect of polar solvents on the photophysical properties of these TPA analogues, the solvent-dependent UV-vis and fluorescence spectra of the compounds were measured in six organic solvents (namely cyclohexane (Cy), tetrahydrofuran (THF), 1,4-dioxane (1,4 Diox), *N*,*N*-dimethylformamide (DMF), acetonitrile (ACN) and dimethyl sulfoxide (DMSO). As shown in Figure S21, as the solvent polarity increases from Cy to DMSO, the UV-vis absorption spectra of **Py2Ph**, **2PyPh**, **PyCz**, and **PyTPE** slightly changed. In particular, the emission has red-shifted *ca*. 62 nm for **Py2Ph**, 50 nm for **2PyPh**, and 72 nm for **PyCz**, respectively (Figure S22). The difference is that the **PyTPE** shows a red-shifted emission from blue (447 nm) to green (505 nm) as the solvent polarity increasing from Cy to ACN, while in DMSO solvent, the **PyTPE** shows a weak emission with a blue-shifted emission peak at 423 nm compared to in ACN. We infer that maybe the AIEgen **PyTPE** shows a better solubility in DMSO than in the other solvents, leading to the emission originating from the pyrene moiety. Therefore, the four compounds show a clear solvatochromic effect, with a pull-push molecular structure. In addition, the relationship between the Stokes shift (Δ_{vst}) and the solvent parameter ($\Delta f(\varepsilon,n)$) was determined by a Lippert–Mataga plot (Figure S23,Table S3).[28]

Theoretical Calculations

To understand the effect of electronic structure on the optical properties of these molecules, the ground state geometry conformation has been optimized by density

functional theory (DFT) calculations at the B3LYP/6-311G (d, p) level [29] for **Py2Ph**, **2PyPh**, **PyCz**, and **PyTPE**. The highest occupied molecular orbital (HOMO) and lowest unoccupied molecular orbital (LUMO) energy levels are charted in Figure S35. The HOMOs of **Py2Ph** and **2PyPh** are almost delocalized across the entire molecules, while the HOMOs of **PyCz** and **PyTPE** are mainly distributed in the phenyl ring and carbazole or partial TPE units, respectively. The LUMO of the four molecules **Py2Ph**, **2PyPh**, **PyCz**, and **PyTPE** are almost entirely distributed over the pyrene unit, indicating that the pyrene ring mainly acts as a weak electron-withdrawing group in these compounds. The aniline, carbazole or TPE units are regarded as electron-donating groups, respectively. The (particle) separated HOMO and LUMO energy levels may contribute to an ICT process in polar solvents, resulting in significant red-shifted emissions via reducing the energy band gaps. This result is consistent with the solvatochromic effects. Thus, the pyrene-based TPA analogues with a D-A structure can undergo a typical ICT transition.

X-ray single crystal diffraction analysis

Three suitable crystals of the pyrene-based fluorophores **Py2Ph**, **PyCz**, and **PyTPE** for X-ray measurements were cultivated in a mixture of THF and hexane solvents. However, attempts to prepare crystals of **2PyPh** were unsuccessful. The key crystallographic information for these crystals is summarized in Table S1. The crystal **Py2Ph** belongs to the monoclinic system with a space group of $P2_1$. As shown in Figure 4A, the pyrene derivative containing diphenylamine has a highly distorted conformation between the pyrene ring and the phenyl, to form a large dihedral angle of 89.71° and 77.72°, respectively. In the packing of the structure, the pyrene is arranged in a head-to-tail herringbone pattern along the *a*-axis, and each phenyl ring was fixed by C-H···π bonds (C9-H9···C26=2.881 Å) with a neighboring pyrene unit. On the other hand, the diphenylamine units adopt a heat-to-head conformation and the phenyl rings are also connected by C-H···π bonds (C19-H19···C28=2.865 Å) along the *c*-axis. In addition, the pyrene ring adopts a slipped π-π stacking in a head-to-head mode along the *b*-axis, and

the centroid-to-centroid distance between pyrenes is 7.268 Å (Figure 4 and Figure S18). This J-aggregation mode is contributing to a larger red-shifted emission peak.

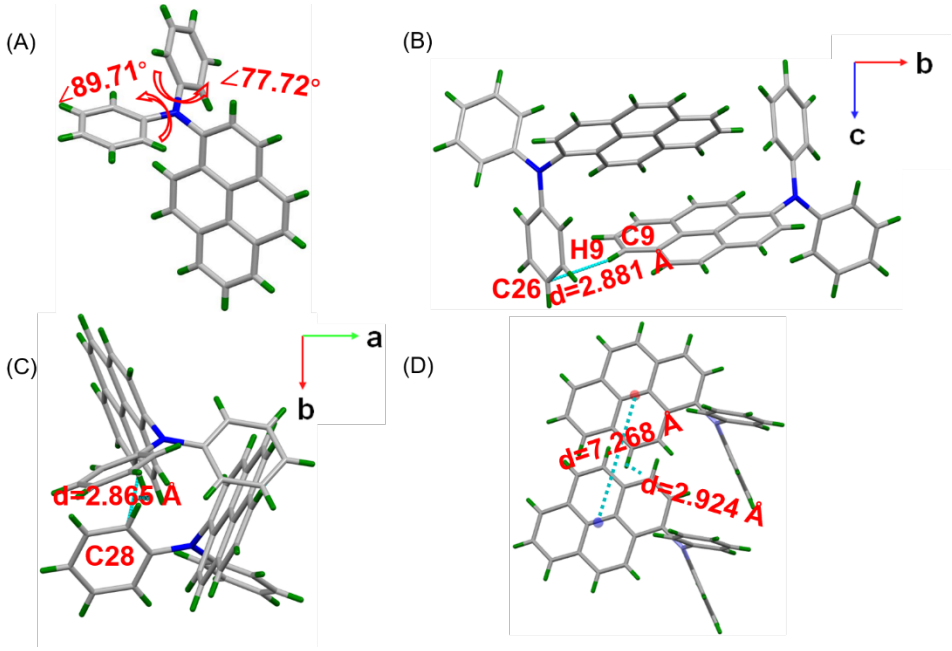

Figure 4. (A) X-ray single crystal structure of **Py2Ph**. The packing structure of **Py2Ph** connected by C-H···π interaction along (B) the *a*-axis and (C) the *c*-axis; (D) J-aggregation mode of **Py2Ph**.

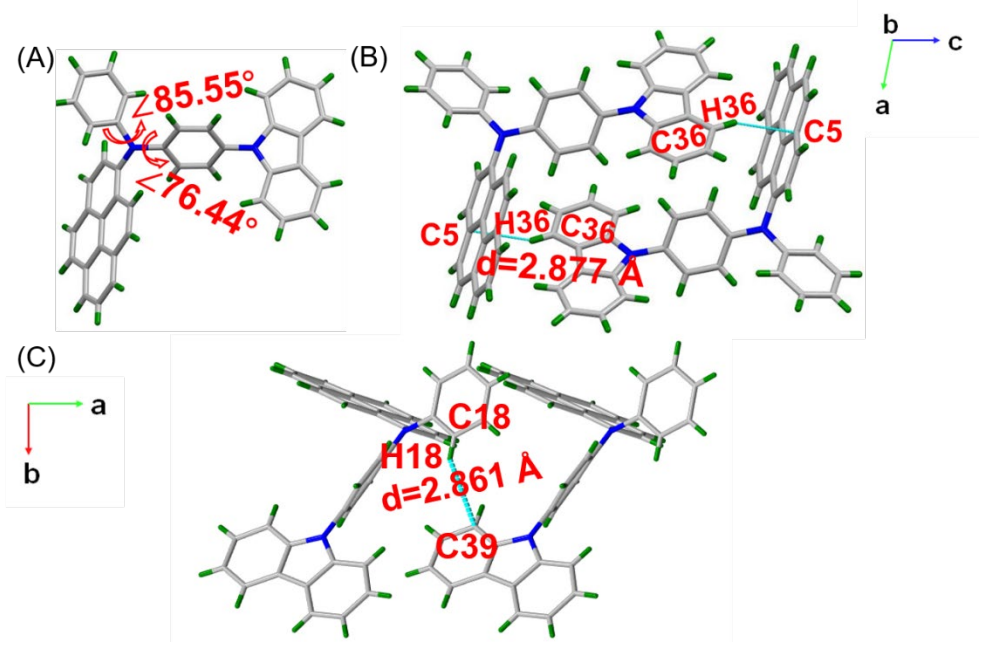

Figure 5. (A) X-ray single crystal structure of **PyCz**. The packing structure of **PyCz** connected by C-H···π interaction along (B) *b*-axis and (C) *c*-axis.

Compound **PyCz** crystallized in the monoclinic space group *P2₁/c*, and the asymmetric unit contains four molecules of **PyCz.** As shown in Figure 5B, the pyrene ring, phenyl and carbazole unit are not co-planar but adopt a 3D molecular configuration, and the pyrene is almost perpendicular with one phenyl ring with a dihedral angle of 85.55°. The dihedral angle between the pyrene and the phenyl ring (connected with carbazole unit) is 76.64°. and the dihedral angle formed between the phenyl ring and carbazole unit is 57.77°, respectively. The molecular packing is dominating by several weak C-H···π interactions (C36-H36···C5=2.877 Å and C18-H18···C39=2.861 Å). There are also two packing modes in the crystal, depending on the interaction of the C-H···π bonds between adjacent molecules. One is the molecules arrange in head-to-tail packing along the *c*-axis, and the other has molecules adopting a ladder-shaped arrangement along the *b*-axis. The centroid-to-centroid distance between the two pyrene cores is 7.989Å. No π-π stacking is observed in the crystal **PyCz**, indicating that the stereoscopic effect induced by the bulky group can contribute to inhibiting the π-π stacking (Figure 5 and Figure S19).

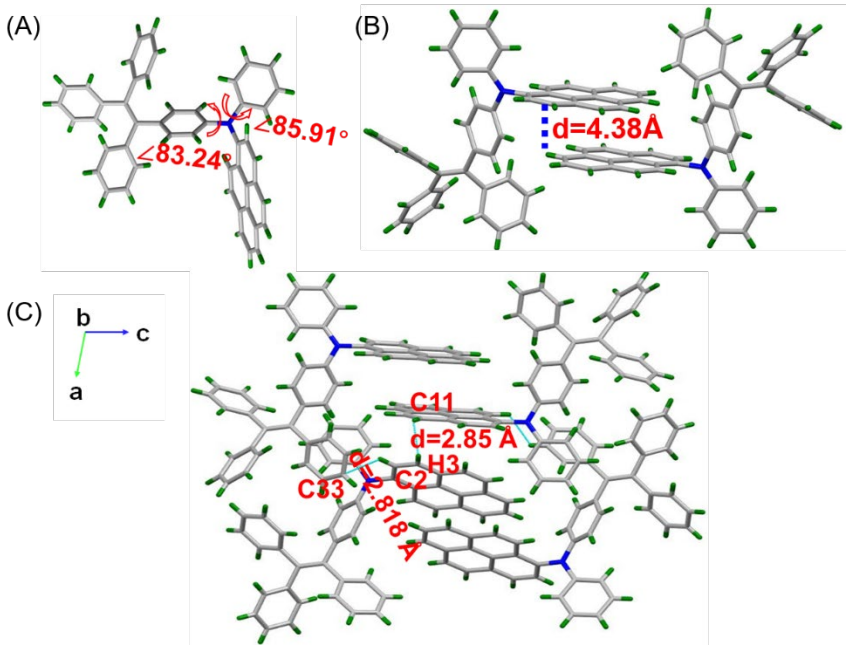

Figure 6. (A) X-ray crystal structure of **PyTPE**; (B) face-to-face π-π stacking of in packing structure along (C) the *b*-axis and multiple weak C–H···π interactions between adjacent molecules with a distance of *ca*. 2,22 Å and 2.85 Å.

On the other hand, compound **PyTPE** is monoclinic with the space group $P2_1/c$. The asymmetric unit of **PyTPE** contains four molecules and a crystallized disordered hexane molecule. The **PyTPE** structure containing the TPE unit also has a highly distorted conformation between the pyrene ring, phenyl and TPE unit. The dihedral angle between the pyrene and the phenyl ring is 83.24°, and the dihedral angle between the pyrene and the phenyl ring from one of the TPE unit is 85.91°, respectively (Figure 6A). The molecules arrange in a head-to-tail stacking pattern and the pyrene ring adopts face-to-face π-π stacking to form a dimer with the H-aggregation model along the *c*-axis, with a distance of *ca*. 3.461 Å. The centroid-to-centroid distance between the adjacent pyrenes is 4.384 Å (Figure 6B), and the pairs of dimers further pack in a herringbone motif through several C-H···π bonds (C2-H2···C33=2.818 Å and C3-H3 ···C11=2.85 Å), indicating the presence of strong intermolecular interactions in this crystal lattice (Figure 6C and Figure S20). This result is consistent with its emission behavior, which shows a relatively large red-shifted emission (24 nm) in the solid state compared to in solution.

Mechanochromism Experiments

In general, TPE-based compounds with AIE characteristics tend to exhibit mechanoluminescence [30] /mechanochromism [31] (ML/MC) properties under mechanical stimulation, which mainly originates from the molecular packing patterns or changing the molecular configuration. To test the ML/MC properties of these four pyrene-based TPE analogues, the solid-state emission behavior was investigated before and after grinding. The compounds **Py2Ph**, **2PyPh** and **PyTPE** exhibit bright emission in the crystal state. After grinding, the maximum emission peak was slightly blue-shifted to 490 nm (**Py2Ph**), 482 nm (**2PyPh**) and 492 nm (**PyTPE**) respectively (Figure S31-S34). The powder X-ray diffraction resulting show that the diffraction peaks have slightly change, indicated that the molecular packing did not change much after grinding.

However, after grinding, the emission intensity of compounds **Py2Ph, PyCz a**nd **2PyPh** has increased compared to the original sample, while the compound **PyTPE** show a decreased fluorescence intensity (Figure S31-S34). The former may be ascribed to their crystal structure; the substituent rotation has been fixed via the intermolecular interactions in this 3D structure, resulting in a rigid molecular structure and the molecule **Py-TPE** tends to form *H*-aggregation after grinding, leading to a blue-shifted emission. [32] In addition, the compound **Py2Ph** also showed an obvious mechanoluminescence phenomenon under mechanical stimuli (Figure 7 and Video S1). The emission color is similar to its photoluminescence, indicating that the electron was transferred from the same excited state. [33]

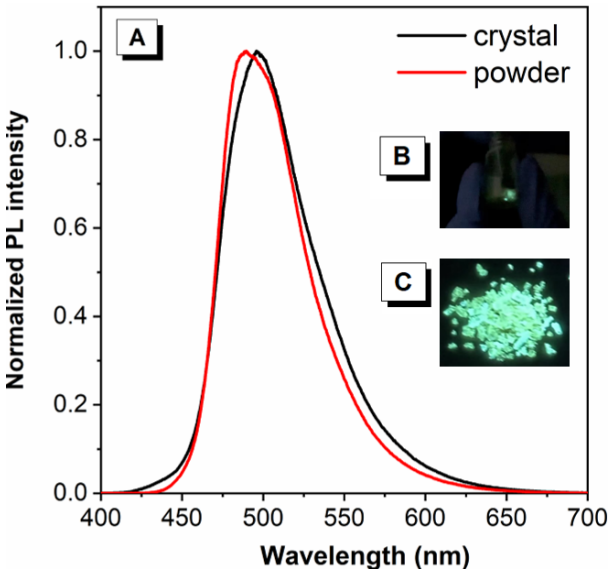

Figure 7. (A) The PL spectrum of **Py2Ph** before and after grinding; (B) ML photo of **Py2Ph** samples obtained through mild mechanical stimulation in the dark; (C) fluorescence photograph of compound **Py2Ph** under 365 nm ultraviolet light irradiation.

Fabrication of OLED Devices

Considering their high thermal stability and good solid-state fluorescence properties, the pyrene-based TPA analogues **PyCz** and **PyTPE** were selected as emitting layers (EML) for fabricating the non-doped OLED devices D1 and D2, with configurations of

ITO/HATCN (5 nm)/TAPC(50 nm)/TCTA (5 nm)/mCP (5 nm)/ EML (20 nm)/TmPyPB (30 nm)/LiF (1 nm)/Al. 1,4,5,8,9,11-Hexaazatriphenylene-hexacarbonitrile (HATCN), di-(4-(*N*,*N*-ditolyl-amino)-phenyl)cyclohexane (TAPC) and tris(4-carbazoyl-9 ylphenyl)amine (TCTA) were used as the hole injection layer, the hole-transporting layer and the electron-blocking layer, respectively. 1,3,5-Tris(3-pyridyl-3-phenyl)benzene (TmPyPB) was used as the electron-transporting layer (ETL) in the construction of devices D1 and D2, while mCP serves as the exciton blocking layers. The energy level diagram, and electroluminescent (EL) performance of the non-doped OLED devices D1 and D2 are shown in Figures 8A–C, and the key EL parameters are summarized in Table 2. The turn-on voltage (V_{on}) of the devices D1 and D2 are 3.0 and 3.1 V, respectively, and both devices emit stable blue light with maximum EL peaks at 470 nm (CIE: x = 0.137, y = 0.158) for D1 and 474 nm (CIE: x = 0.151, y = 0.229) for D2 and maximum luminescence of 12710 cd m^{-2} and 9185 cd m^{-2}, respectively. The maximum current efficiency (η_C), power efficiency (η_P) and external quantum efficiency (η_{ext}) are 5.4 cd A^{-1}, 5.2 lm W^{-1} and 4.4% for D1 and 4.2 cd A^{-1}, 4.0 lm W^{-1} and 2.7% for D2, respectively. The low turn on-voltage and excellent EL properties may contribute to the balance of carrier transport. Furthermore, the efficiency of the roll-off at 1000 cd m^{-2} (RO_{1000}) has been calculated by the equation $RO_{1000} = [(\eta_{Cmax} - \eta_{C1000})/ \eta_{Cmax}]\times100\%$, and the calculated RO_{1000} of the non-doped OLED devices are 9.26% for D1 and 19.0% for D2, respectively. On comparing these non-doped OLED devices, D1 using **PyCz** as the light-emitting layer shows better EL characteristics than D2 using **PyTPE** as the light-emitting layer. This may be due to a more rigid molecular structure decorated by the hole transport of carbazole unit.

Table 2. EL performance of blue OLEDs based on Device **1** and Device **2**

Device	λ_{EL} (nm)	L (cd m^{-2})[a)]	Voltage	η_C (cd A^{-1})[a)]	η_P (lm W^{-1})[a)]	η_{ext} (%)[a)]	CIE (x, y)[c)]
			V_{on}[b)]/1000 cd m^{-2}	maximum value / at 1000 cd m^{-2}			
D1	470	12710	3.0/3.9	5.4/4.9	5.2/3.9	4.4/4.0	(0.137,0.158)
D2	474	9185	3.1/3.9	4.2/3.4	4.0/2.7	2.7/2.2	(0.151,0.229)

Configuration:
ITO/HATCN (5 nm)/TAPC (50 nm)/TCTA (5 nm)/mCP (5 nm)/PyCz or PyTPE (20 nm)/TmPyPB (30 nm)/LiF (1 nm)/Al

[a)] The luminescence (L), current efficiency (η_c), power efficiency (η_P), and external

quantum efficiency (η_{ext}) of the devices: maximum values/ values at 1000 cd m^{-2}; [b] Turn-on voltage at 1 cd m^{-2}; [c] CIE coordinates at 1000 cd/m^2.

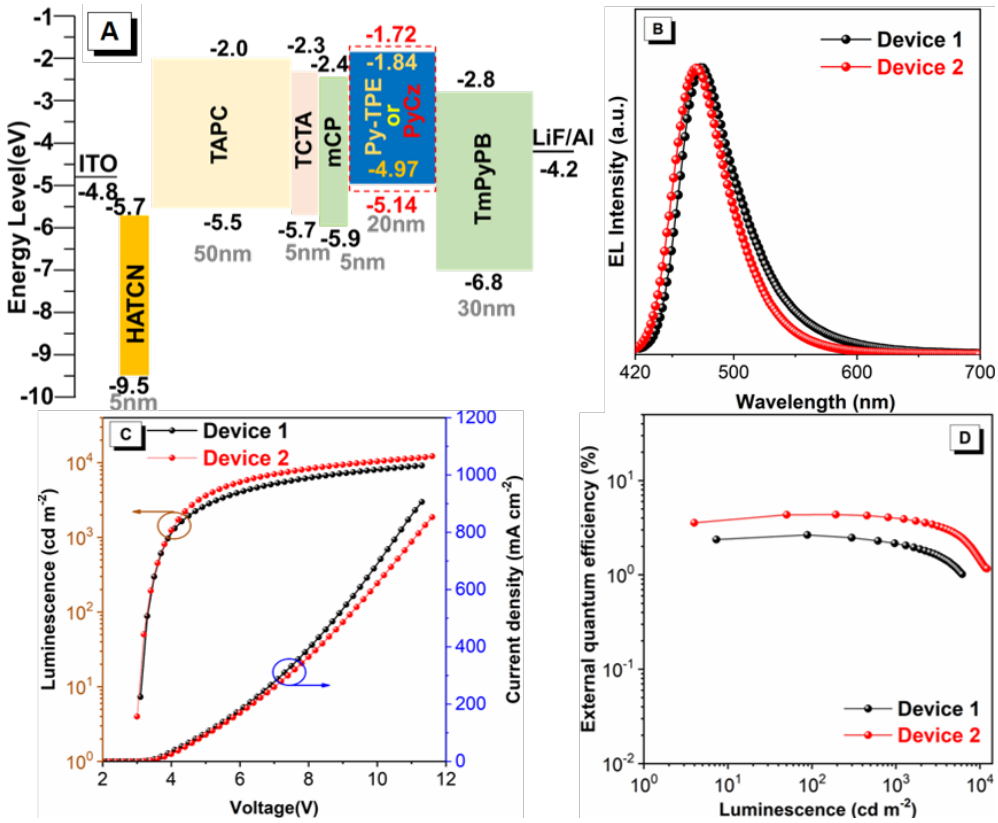

Figure 8. The schematic energy level diagram of related materials used in the fabrication of the OLED devices A) for Device **1** and Device **2**; B) EL spectra recorded at 1000 cd m−2; C) luminance–voltage–current density (L–V–J) characteristics; D) external quantum efficiency with the current density.

Conclusions

In summary, four novel pyrene-based TPA analogues were synthesized and their structure and properties have been discussed. To regulate the molecular structure and steric effects, one of the phenyl rings of TPA was replaced by pyrene, phenylcarbazole, and tetraphenylethylene, respectively. The series of TPA analogues containing a pyrene unit exhibit different emission behavior. The compounds **Py2Ph**, **2PyPh** and **PyCz** are ACQ fluorophores, and the **PyTPE** is AIE-active. Moreover, the **Py2Ph** exhibits a mechanoluminescence phenomenon, while the other compounds show slight emission changes under mechanical stimuli. The compounds **PyCz** and **PyTPE**

were utilized for non-doped OLEDs, and due to the rigid molecular structure of **PyCz**, the OLED devices exhibit better EL properties with a maximum emission peak at 470 nm and a maximum external quantum efficiency of 4.4%. This article offer an opportunities for the construction of high-performance pyrene-based luminescent materials for OLED applications.

CRediT authorship contribution statement

Xinyi Song: Investigation, resources and visualization. Min Wang: Investigation and visualization, Wei Liu: Investigation, Heng Zheng: Investigation, Carl Redshaw: Writing - review & editing. Xing Feng: Data curation, conceptualization, Writing-original draft, supervision, project administration. Zujin Zhao: Data curation, Writing-original draft, Ben Zhong Tang: Supervision.

Declaration of competing interest

There are no conflicts to declare.

Acknowledgements

X. Song and M. Wang contributed equally to this work. This work was supported by the National Natural Science Foundation of China (21975054), Natural Science Foundation of Guangdong Province of China (2019A1515010925), Shenzhen Key Laboratory of Functional Aggregate Materials (ZDSYS20211021111400001), the Science Technology Innovation Commission of Shenzhen Municipality (KQTD20210811090142053, JCYJ20220818103007014) Guangdong Provincial Key Laboratory of Information Photonics Technology (2020B121201011), the Open Fund of Guangdong Provincial Key Laboratory of Luminescence from Molecular Aggregates, Guangzhou 510640, China (South China University of Technology) (2019B030301003), Science and Technology Planning Project of Hunan Province (2018TP1017), CR thanks the University of Hull for support.

References

[1] Yang, Z.; Mao, Z.; Xie, Z.; Zhang, Y.; Liu, S.; Zhao, J.; Xu, J.; Chi, Z.; Aldred, M. P. Recent advances in organic thermally activated delayed fluorescence materials. *Chem. Soc. Rev.* **2017**, *46*, 915-1016.

[2] Xu, Y.; Xu, P.; Hu, D.; Ma, Y. Recent progress in hot exciton materials for organic light-emitting diodes. *Chem. Soc. Rev.* **2021**, *50*, 1030-1069.

[3] Jhang, S. J.; Pandidurai, J.; Chu, C. P.; Miyoshi, H.; Takahara, Y.; Miki, M.; Sotome, H.; Miyasaka, H.; Chatterjee, S.; Ozawa, R.; Ie, Y.; Hisaki, I.; Tsai, C. L.; Cheng, Y. J.; Tobe, Y. s-Indacene Revisited: Modular Synthesis and Modulation of Structures and Molecular Orbitals of Hexaaryl Derivatives. *J. Am. Chem. Soc.* **2023**, *145*, 4716-4729.

[4] Tu, Y.; Zhao, Z.; Lam, J. W. Y.; Tang, B. Z. Aggregate Science: Much to Explore in the Meso World. *Matter.* **2021**, *4*, 338-349.

[5] Luo, J.; Xie, Z.; Lam, J. W.; Cheng, L.; Chen, H.; Qiu, C.; Kwok, H. S.; Zhan, X.; Liu, Y.; Zhu, D.; Tang, B. Z. Aggregation-induced emission of 1-methyl-1,2,3,4,5-pentaphenylsilole. *Chem. Commun.* **2001**, 1740-1741.

[6] Mei, J.; Leung, N. L.; Kwok, R. T.; Lam, J. W.; Tang, B. Z. Aggregation-Induced Emission: Together We Shine, United We Soar! *Chem. Rev.* **2015**, *115*, 11718-11940.

[7] Yang, J.; Fang, M.; Li, Z. Organic luminescent materials: The concentration on aggregates from aggregation-induced emission. *Aggregate* **2020**, *1*, 6-18.

[8] Peng, Q.; Shuai, Z. Molecular mechanism of aggregation-induced emission. *Aggregate* **2021**, *2*, e91.

[9] Wang, X.; Zhang, J.; Mao, X.; Liu, Y.; Li, R.; Bai, J.; Zhang, J.; Redshaw, C.; Feng, X.; Tang, B. Z. Intermolecular Hydrogen-Bond-Assisted Solid-State Dual-Emission Molecules with Mechanical Force-Induced Enhanced Emission. *J. Org. Chem.* **2022**, *87*, 8503-8514.

[10] Zhang, y.-p.; Teng, Q.; Yang, Y.-S.; Cao, J.-Q.; Xue, J.-J. Aggregation-Induced Emission Properties of Triphenylamine Chalcone Compounds. *J. Fluoresc.* **2021**,

31, 807-815.

[11] Wen, Z.; Yang, T.; Zhang, D.; Wang, Z.; Dong, S.; Xu, H.; Miao, Y.; Zhao, B.; Wang, H. A multifunctional luminescent material based on quinoxaline and triphenylamine groups: polymorphism, mechanochromic luminescence, and applications in high-efficiency fluorescent OLEDs. *J. Mater. Chem. C* **2022**, *10*, 3396-3403.

[12] Li, T.; Wu, Y.; Cai, W.; Wang, D.; Ren, C.; Shen, T.; Yu, D.; Qiang, S.; Hu, C.; Zhao, Z.; Yu, J.; Peng, C.; Tang, B. Z. Vision Defense: Efficient Antibacterial AIEgens Induced Early Immune Response for Bacterial Endophthalmitis. *Adv. Sci.* **2022**, *9*, e2202485.

[13] Han, X.; Ge, F.; Xu, J.; Bu, X. H. Aggregation-induced emission materials for nonlinear optics. *Aggregate* **2021**, *2*, e28.

[14] Li, Y.; Wang, W.; Zhuang, Z.; Wang, Z.; Lin, G.; Shen, P.; Chen, S.; Zhao, Z.; Tang, B. Z. Efficient red AIEgens based on tetraphenylethene: synthesis, structure, photoluminescence and electroluminescence. *J. Mater. Chem. C* **2018**, *6*, 5900-5907.

[15] Zhou, L.; Chen, W.-C.; Tan, J.-H.; Ji, S.; Yang, Q.; Mu, Y.; Zhang, H.-L.; Zhao, J.; Huo, Y.; Lee, C.-S. Versatile azaryl-ketone-based blue AIEgens for efficient organic light-emitting diodes. *Dyes Pigm.* **2021**, *195,* 109729.

[16] Figueira-Duarte, T. M.; Mullen, K. Pyrene-based materials for organic electronics. *Chem. Rev.* **2011**, *111*, 7260-7314.

[17] Mateo-Alonso, A. Pyrene-fused pyrazaacenes: from small molecules to nanoribbons. *Chem. Soc. Rev.* **2014**, *43*, 6311-6324.

[18] Crawford, A. G.; Dwyer, A. D.; Liu, Z.; Steffen, A.; Beeby, A.; Palsson, L. O.; Tozer, D. J.; Marder, T. B. Experimental and theoretical studies of the photophysical properties of 2- and 2,7-functionalized pyrene derivatives. *J. Am. Chem. Soc.* **2011**, *133*, 13349-13362.

[19] Islam, M. M.; Hu, Z.; Wang, Q. S.; Redshaw, C.; Feng, X. Pyrene-based aggregation-induced emission luminogens and their applications. *Mater. Chem. Front.* **2019**, *3*, 762-781.

[20] Feng, X.; Hu, J. Y.; Redshaw, C.; Yamato, T. Functionalization of Pyrene To Prepare Luminescent Materials-Typical Examples of Synthetic Methodology. *Chem. Euro. J.* **2016**, *22*, 11898-11916.

[21] Mao, X. Y.; Xie, F. L.; Wang, X. H.; Wang, Q. S.; Qiu, Z. P.; Elsegood, M. R. J.; Bai, J.; Feng, X.; Redshaw, C.; Huo, Y. P.; Hu, J. Y.; Chen, Q. New Quinoxaline-Based Blue Emitters: Molecular Structures, Aggregation-Induced Enhanced Emission Characteristics and OLED Application. *Chin. J. Chem.* **2021**, *39*, 2154-2162.

[22] Wang, X. H.; Wang, L. R.; Mao, X. Y.; Wang, Q. S.; Mu, Z. F.; An, L.; Zhang, W.; Feng, X.; Redshaw, C.; Cao, C. Y.; Qin, A. J.; Tang, B. Z. Pyrene-based aggregation-induced emission luminogens (AIEgens) with less colour migration for anti-counterfeiting applications. *J. Mater. Chem. C* **2021**, *9*, 12828-12838.

[23] Yang, S. W.; Elangovan, A.; Hwang, K. C.; Ho, T. I. Electronic polarization reversal and excited state intramolecular charge transfer in donor/acceptor ethynylpyrenes. *J. Phys. Chem. B* **2005**, *109*, 16628-16635.

[24] Feng, X.; Qi, C.; Feng, H. T.; Zhao, Z.; Sung, H. H. Y.; Williams, I. D.; Kwok, R. T. K.; Lam, J. W. Y.; Qin, A.; Tang, B. Z. Dual fluorescence of tetraphenylethylene-substituted pyrenes with aggregation-induced emission characteristics for white-light emission. *Chem. Sci.* **2018**, *9*, 5679-5687.

[25] Divac, V. M.; Sakic, D.; Weitner, T.; Gabricevic, M. Solvent effects on the absorption and fluorescence spectra of Zaleplon: Determination of ground and excited state dipole moments. *Spectrochim. Acta. A. Mol. Biomol. Spectrosc.* **2019**, *212*, 356-362.

[26] Stephens, P. J.; Devlin, F. J.; Chabalowski, C. F.; Frisch, M. J. Ab Initio Calculation of Vibrational Absorption and Circular Dichroism Spectra Using Density Functional Force Fields. *J. Phys. Chem. C* **2002**, *98*, 11623-11627.

[27] Yang, Z.; Chi, Z.; Mao, Z.; Zhang, Y.; Liu, S.; Zhao, J.; Aldred, M. P.; Chi, Z. Recent advances in mechano-responsive luminescence of tetraphenylethylene derivatives with aggregation-induced emission properties. *Mater. Chem. Front.* **2018**, *2*, 861-890.

[28] Nie, Y.; Zhang, H.; Miao, J.; Zhao, X.; Li, Y.; Sun, G. Synthesis, aggregation-induced emission and mechanochromism of a new carborane-tetraphenylethylene hybrid. *J. Organomet. Chem.* **2018**, *865*, 200-205.

[29] Deng, Y.; Yuan, W.; Jia, Z.; Liu, G. H- and J-aggregation of fluorene-based chromophores. *J. Phys. Chem. B* **2014**, *118*, 14536-14545.

[30] SAINT and APEX 2. Software for CCD diffractometers. **2015**

[31] Sheldrick, G. M. *Acta Crystallogr A Found Adv* **2015**, *71*, 3-8.

[32] Sheldrick, G. M. *Acta Crystallogr A* **2008**, *64*, 112-122.

[33] Gu, J.; Li, Z.; Li, Q. *Coord Chem Rev* **2023**, *475*.-something missing here.